

Numerical continuation of spiral waves in heteroclinic networks of cyclic dominance

Cris R. Hasan,

School of Mathematical Sciences, University College Cork, Ireland
rhasan@ucc.ie

Hinke M. Osinga, Claire M. Postlethwaite

Department of Mathematics, The University of Auckland, New Zealand

and Alastair M. Rucklidge

School of Mathematics, University of Leeds, UK

Abstract

Heteroclinic-induced spiral waves may arise in systems of partial differential equations that exhibit robust heteroclinic cycles between spatially uniform equilibria. Robust heteroclinic cycles arise naturally in systems with invariant subspaces and their robustness is considered with respect to perturbations that preserve these invariances. We make use of particular symmetries in the system to formulate a relatively low-dimensional spatial two-point boundary-value problem in Fourier space that can be solved efficiently in conjunction with numerical continuation. Our numerical set-up is formulated initially on an annulus with small inner radius, and Neumann boundary conditions are used on both inner and outer radial boundaries. We derive and implement alternative boundary conditions that allow for continuing the inner radius to zero and so compute spiral waves on a full disk. As our primary example, we investigate the formation of heteroclinic-induced spiral waves in a reaction-diffusion model that describes the spatiotemporal evolution of three competing populations in a two-dimensional spatial domain—much like the Rock–Paper–Scissors game. We further illustrate the efficiency of our method with the computation of spiral waves in a larger network of cyclic dominance between five competing species, which describes the so-called Rock–Paper–Scissors–Lizard–Spock game.

1 Introduction

In dynamical systems, a heteroclinic cycle is a set of trajectories that connect equilibria in a topological circle (Guckenheimer & Holmes, 1988; Krupa, 1997). In general, such a cycle does not persist under perturbation, unless the dynamical system has a special structure. More precisely, this phenomenon occurs in systems with special properties that allow for the existence of a sequence of invariant subspaces. A heteroclinic cycle is called robust, or structurally stable, when it persists under small perturbations that preserve this special structure. In one of its simplest forms, a robust heteroclinic cycle involves three saddle equilibria and their connecting

trajectories in a system for which the equilibria are pairwise contained in an invariant subspace. This situation often occurs in population models and cyclic interactions are known to provide a naturally selective coexistence mechanism for interspecific competition between three subpopulations, including morphs of the side-blotched lizard (Sinervo & Lively, 1996; Sinervo et al., 2000), coral reef invertebrates (Jackson & Buss, 1975; Taylor & Aarssen., 1990), and strains of *Escherichia coli* (Kerr et al., 2002; Kirkup & Riley, 2004). The dynamics near a robust three-equilibrium heteroclinic cycle also emulates the famous children’s game of Rock–Paper–Scissors, where Rock crushes Scissors, Scissors cut Paper and Paper wraps Rock.

The focus of this paper is on the computation of spiral waves arising from cyclic interactions between competing populations in the presence of spatial diffusion. We assume that this system is modelled by a system of partial differential equations (PDEs) given in vector form as

$$\mathbf{U}_t = \mathbf{f}(\mathbf{U}) + \mathbf{U}_{xx} + \mathbf{U}_{yy}. \quad (1)$$

Here, $\mathbf{U}(x, y, t) \in \mathbb{R}^m$ represents m different species, $\mathbf{f}: \mathbb{R}^m \rightarrow \mathbb{R}^m$ is a sufficiently smooth function expressing the nonlinear kinetics (i.e., local species interactions), and the spatial derivatives $\mathbf{U}_{xx} + \mathbf{U}_{yy}$ are the Laplacian terms modelling diffusion. We are interested in a specific class of (1) that satisfies the following assumption:

Assumption 1.1

We assume that, in the absence of spatial variation and diffusion terms, (1) admits an attracting, robust heteroclinic cycle between equilibria solutions. Furthermore, we assume that \mathbf{f} is invariant under cyclic permutations of its arguments.

Systems of the form (1) that satisfy Assumption 1.1 describe a large class of problems that feature heteroclinic cycles with permutation symmetries (i.e., cyclic symmetries). Well-known examples of this class include those arising in equivariant bifurcation theory (e.g., the three-variable Guckenheimer–Holmes cycle (Guckenheimer & Holmes, 1988) and the four-variable Field–Swift cycle (Field & Swift, 1991)); population models (e.g., the May–Leonard model (May & Leonard, 1975) and other higher-dimensional generalisations of Lotka–Volterra type); and also those that can appear in other mathematical modelling problems (e.g., the example of Proctor & Jones (1988) from fluid mechanics). Note that the diffusion coefficients for all state variables in system (1) are equal; this is necessary to preserve the permutation symmetry. If we perturb the system by breaking this symmetry, for example by choosing unequal diffusion coefficients slightly different from 1, we expect the dynamics to be similar, although the computations will be more expensive.

Remark 1.1 *The computational method presented here can be generalized to compute spiral waves in any reaction–diffusion system of the general form (1), but in the absence of the cyclic symmetry given by Assumption 1.1 the computational cost will then likely be larger.*

Figure 1 shows an example of a spiral wave for the simplest case of system (1) with $m = 3$; the precise equations are given in equation (2) in the next section. The species are represented in terms of their scaled densities a , b and c at an arbitrarily chosen instant in time. With $m = 3$ there exists

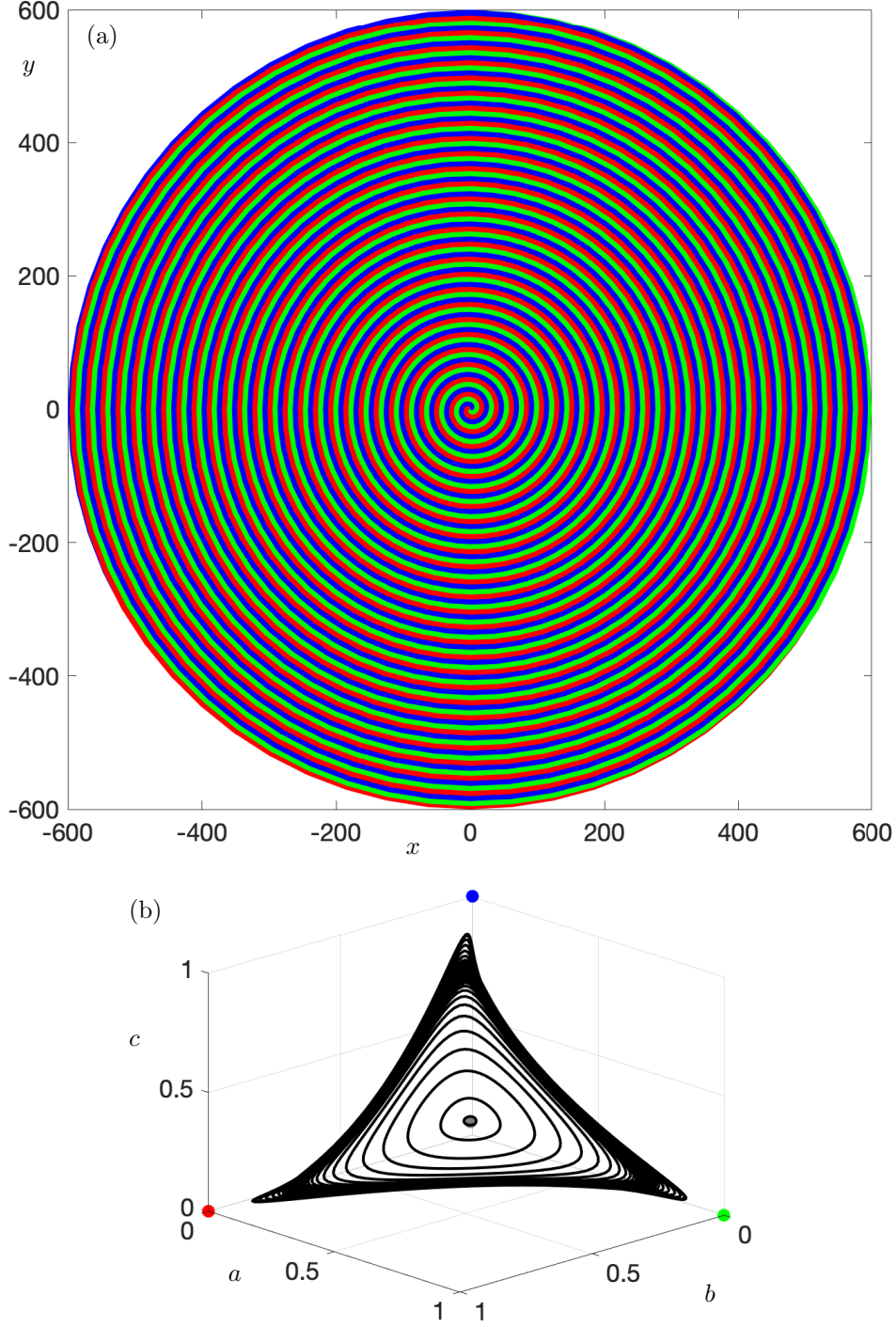


Figure 1: A large spiral wave formed by the three competing species of system (2) with parameters $\sigma = 3.2$ and $\zeta = 0.8$, shown at a fixed moment in time. Panel (a) shows the spiral wave solution on an annulus in the (x, y) -plane; the three different colours represent which of the population densities a , b and c is the largest. Panel (b) shows their distribution in (a, b, c) -space along a selection of concentric circles around the origin in the (x, y) -plane; the smallest and largest circles are the inner and outer boundaries of the computed domain at radii 0.01 and 600, respectively. The grey dot is the coexistence equilibrium and the colored dots are the on-axis equilibria where only one species survives.

only one heteroclinic cycle, formed by connecting orbits between the equilibria $(a, b, c) = (1, 0, 0)$, $(0, 1, 0)$ and $(0, 0, 1)$. There also exists a spatially-uniform coexistence equilibrium $(a, b, c) = \frac{1}{3+\sigma}(1, 1, 1)$, at which all species survive. The spiral wave was computed on an annulus in the (x, y) -plane, centred at the origin, with inner radius 0.01 and outer radius 600. Panel (a) illustrates the spiral wave in the (x, y) -plane with red, green and blue regions indicating the dominance of a , b and c , respectively, that is, which of the three populations, a , b or c is the largest. Panel (b) shows the population densities (black curves) in (a, b, c) -space, where x and y vary along a family of concentric circles around the origin; here, the smallest cycle in (a, b, c) -space corresponds to the inner boundary with radius 0.01 in the (x, y) -plane and the largest corresponds to the outer boundary of the annulus with the very large radius of 600. The grey dot is the coexistence equilibrium and the coloured dots are the on-axis equilibria that are involved in the limiting heteroclinic cycle. The periodic curves in the (a, b, c) -space are centred on a point which is close to, but not exactly at, the coexistence equilibrium, indicating that the core of the spiral at $(x, y) = (0, 0)$ should satisfy $a = b = c \approx \frac{1}{3+\sigma}$. The population densities along the outermost circle accumulate on a periodic solution that comes close to, but remains a finite distance from, each of the three equilibria in turn. This periodic solution is related to the periodic travelling waves found in the one-dimensional version of this problem, and to the underlying heteroclinic cycle (Hasan et al., 2021). In contrast to the almost uniform distribution along the inner circle, the variation of the population densities along the outer circle is non-uniform, with each of the species being close to zero along two thirds of the perimeter.

Most previous approaches for numerical continuation of spirals (Barkley, 1992; Bär et al., 2003; Bordyugov & Engel, 2007; Dodson & Sandstede, 2019) have focussed on systems of reaction–diffusion type, in which a spatially uniform equilibrium solution loses stability in a Hopf (Turing) bifurcation, leading to spiral waves. The spiral waves in our examples have oscillations associated with heteroclinic cycles rather than Hopf bifurcations, so we call these *heteroclinic-induced spirals*. As the radius of the spiral goes to infinity, the system approaches a periodic orbit in the far field that is associated with a heteroclinic bifurcation from the heteroclinic cycle (Postlethwaite & Rucklidge, 2017, 2019; Hasan et al., 2021). The proximity to a heteroclinic cycle makes the continuation the spiral wave a challenge because in the far field, the variables switch fairly abruptly from being nearly zero to being nearly one and back again.

Our method is based on the approach by Bordyugov & Engel (2007), who compute spiral waves in reaction–diffusion systems as a continuation of solutions to a two-point boundary-value problem (BVP) formulated in Fourier space. In systems of heteroclinic networks, when the periodic orbit in the far field approaches the heteroclinic cycle, the rapid switching between episodes of the variables being nearly constant means that a large number of Fourier modes may be necessary. Consequently, the computation of the spiral wave on a large domain requires solving a computationally expensive BVP. We make use of the symmetry of the heteroclinic cycle, imposing phase relations between the Fourier modes, and so obtaining a significant reduction in the dimension of the BVP; the efficiency of this approach is most apparent when a large number of species is considered.

We also aim to study the dynamics on the full disk rather than just on an annulus, which is not

possible using the Neumann boundary conditions suggested by Bordyugov & Engel (2007). More precisely, when taking the inner boundary to zero radius, one encounters a singular Laplacian with such boundary conditions. We derive and implement the correct boundary conditions at the core in order to obtain a bounded Laplacian term in polar coordinates. In this way, we compute the spiral waves on a full disk, as opposed to considering an annulus with a small hole around the origin.

As our primary example, we use the three-species model illustrated in fig. 1 and introduced in the next section. This is the simplest model with a robust heteroclinic cycle and the same model that we studied in Postlethwaite & Rucklidge (2017, 2019) and Hasan et al. (2021), where we focussed on the bifurcation structure of different types of heteroclinic cycles, and the computation of periodic travelling waves. The dynamics of the heteroclinic-induced spiral waves for this model have also been investigated by others (Reichenbach et al., 2008; Szczesny et al., 2013, 2014; Szolnoki et al., 2014), with focus on existence and break-up of the spiral-wave patterns in the presence of small defects, based on analysis and simulation of the full PDE. We chose this three-species competition model as our primary example because the numerical set-up and efficiency gains are already evident for this simple example, and the computations are readily compared with other results from the literature. We also show how to adapt the numerical set-up for the computation of spiral waves in a system of the form (1) with $m = 5$; see already equation (14). This higher-dimensional example not only has a heteroclinic cycle between all five equilibria with only one surviving species, but also one between five equilibria with three surviving species each. We compute spiral waves from both families to emphasise the versatility of our computational method.

This paper is organised as follows. In the next section, we introduce our primary example given by system (1) with $m = 3$ and review the method from Bordyugov & Engel (2007). In section 2.3, we exploit the cyclic symmetry and present a reduced BVP. We discuss the boundary conditions at the core of the spiral waves in section 2.5. In section 3, we present a case study where we explore the properties of spiral waves for our primary example and compare with published results. In section 4, we introduce the system of associated competing population model with cyclic dominance between five species and implement the modified continuation method to compute two families of five-component spiral waves. We conclude the paper with a discussion and final remarks in section 5.

2 Computing spiral waves in the three-species model

The model for heteroclinic-induced spiral waves between three competing populations was first proposed by Reichenbach et al. (2007) and is based on the system of three ordinary differential equations introduced by May & Leonard (1975) as a model of competing populations without spatial structure and diffusion. See (Frey, 2010; Szolnoki et al., 2014) for details and a recent review. The system of partial differential equations (PDEs) is defined in terms of three population

densities $a(x, y, t), b(x, y, t), c(x, y, t) \geq 0$ that are scaled to unity; it is given by

$$\begin{cases} \dot{a} &= a(1 - a - b - c - (\sigma + \zeta)b + \zeta c) + \nabla^2 a, \\ \dot{b} &= b(1 - a - b - c - (\sigma + \zeta)c + \zeta a) + \nabla^2 b, \\ \dot{c} &= c(1 - a - b - c - (\sigma + \zeta)a + \zeta b) + \nabla^2 c. \end{cases} \quad (2)$$

The parameters σ and ζ are non-negative constants that represent removal and replacement rates of two different interacting species, respectively (Szczesny et al., 2013). We used the notation ∇^2 for the Laplace operator ($\frac{\partial^2}{\partial x^2} + \frac{\partial^2}{\partial y^2}$) that models the diffusion on the two-dimensional domain; nonlinearity in the diffusion (Szczesny et al., 2013), is not included in this model. The only nonlinearity is the population kinetics, as defined by the function \mathbf{f} in system (1). Note the cyclic symmetry of the kinetic term: if $(a, b, c) = (d_1, d_2, d_3)$ is a solution to system (2) then the cyclic permutations $(a, b, c) = (d_2, d_3, d_1)$ and $(a, b, c) = (d_3, d_1, d_2)$ are also solutions to this system of PDEs. Furthermore, in the absence of spatial distribution, the coexistence equilibrium point is unstable and all trajectories are attracted to the heteroclinic cycle. Subspaces with one or more population equal to zero are invariant, and hence, this system is of the form (1) and satisfies Assumption 1.1.

Spiral waves for system (2) can be computed with any of the methods described by Barkley (1992), Bär et al. (2003), Bordyugov & Engel (2007) or Dodson & Sandstede (2019). In this section, we only review the numerical continuation method introduced by Bordyugov & Engel (2007), because it forms the basis for our improved approach.

2.1 Spiral waves on an annulus: the Fourier decomposition

The spiral waves for systems of the form (1) are so-called rigidly rotating spirals, which are periodic in time and any shift in time is equivalent to a rotation in space. Furthermore, the centre of rotation, that is, the tip of the spiral, can be anywhere in the (x, y) -plane. To capture the spatiotemporal rotation symmetry, it is convenient to re-write system (1) in polar coordinates, where we define $x = r \cos \phi$ and $y = r \sin \phi$, with $r = 0$ being the tip of the spiral. Then the PDE is given by

$$\mathbf{U}_t = \mathbf{f}(\mathbf{U}) + \mathbf{U}_{rr} + \frac{1}{r}\mathbf{U}_r + \frac{1}{r^2}\mathbf{U}_{\phi\phi}.$$

The next natural step is to assume that the spiral waves rotate at a constant angular frequency ω and introduce the co-rotating variable $\theta = \phi + \omega t$. Then $\frac{\partial}{\partial \phi} \mapsto \frac{\partial}{\partial \theta}$ and $\frac{\partial}{\partial t} \mapsto \omega \frac{\partial}{\partial \theta} + \frac{\partial}{\partial t}$, which leads to the PDE in the co-rotating frame of reference:

$$\mathbf{U}_t = \mathbf{f}(\mathbf{U}) + \mathbf{U}_{rr} + \frac{1}{r}\mathbf{U}_r + \frac{1}{r^2}\mathbf{U}_{\theta\theta} - \omega \mathbf{U}_\theta.$$

A rigid spiral wave with angular frequency ω and temporal period $T = 2\pi/\omega$ is a stationary solution of this PDE, i.e., it satisfies

$$\mathbf{f}(\mathbf{U}) + \mathbf{U}_{rr} + \frac{1}{r}\mathbf{U}_r + \frac{1}{r^2}\mathbf{U}_{\theta\theta} - \omega \mathbf{U}_\theta = 0. \quad (3)$$

Since spiral wave solutions are periodic in θ , that is, $\mathbf{U}(r, \theta) = \mathbf{U}(r, \theta + 2\pi)$, they can be expressed as a Fourier series expansion with respect to the second argument. We assume that the Fourier coefficients converge rapidly so that only a finite number of modes is sufficient to approximate $\mathbf{U}(r, \theta)$. Using N Fourier modes, where N is assumed to be even, we define N uniformly spaced angles $\theta = 2\pi \frac{n}{N}$, with $n = 0, 1, \dots, N-1$, and approximate the spiral wave as

$$\mathbf{U}(r, 2\pi \frac{n}{N}) = \sum_{k=0}^{N-1} \hat{\mathbf{U}}(r, k) e^{2\pi i \frac{kn}{N}}.$$

Here, each $\hat{\mathbf{U}}(r, k)$, with $k = 0, 1, \dots, N-1$, is a vector of (complex-valued) Fourier coefficients associated with the k th Fourier mode, and it is defined as

$$\hat{\mathbf{U}}(r, k) = \frac{1}{N} \sum_{n=0}^{N-1} \mathbf{U}(r, 2\pi \frac{n}{N}) e^{-2\pi i \frac{kn}{N}}.$$

The goal is to solve the PDE in the co-rotating frame (3) with respect to the unknown Fourier coefficient vectors $\hat{\mathbf{U}}(r, k)$ and the unknown angular frequency ω . To this end, we need the Fourier transform of the nonlinear kinetics function \mathbf{f} . For the case of the three-species population model (2), the nonlinear kinetics is quadratic and Fourier coefficients $\hat{\mathbf{f}}(r, k)$, for $k = 0, 1, \dots, N-1$, of the discretised Fourier approximation

$$\mathbf{f}\left(\mathbf{U}(r, 2\pi \frac{n}{N})\right) = \sum_{k=0}^{N-1} \hat{\mathbf{f}}(r, k) e^{2\pi i \frac{kn}{N}}$$

can formally be expressed as a sum of convolutions in terms of the Fourier transforms \hat{a} , \hat{b} and \hat{c} of the population densities a , b and c , respectively. More precisely,

$$\hat{\mathbf{f}}(r, k) = \begin{pmatrix} \hat{a} - \hat{a} * \hat{a} - (1 + \sigma + \zeta) \hat{a} * \hat{b} - (1 - \zeta) \hat{a} * \hat{c} \\ \hat{b} - \hat{b} * \hat{b} - (1 + \sigma + \zeta) \hat{b} * \hat{c} - (1 - \zeta) \hat{b} * \hat{a} \\ \hat{c} - \hat{c} * \hat{c} - (1 + \sigma + \zeta) \hat{c} * \hat{a} - (1 - \zeta) \hat{c} * \hat{b} \end{pmatrix} (r, k), \quad (4)$$

where, for example, the convolution $\hat{a}(r, k) * \hat{b}(r, k)$ is calculated as a fast Fourier transform (FFT) of the product $a(r, \theta) b(r, \theta)$ obtained from the inverse fast Fourier transform (IFFT) of the individual Fourier coefficients $\hat{a}(r, k)$ and $\hat{b}(r, k)$; in other words,

$$\hat{a}(r, k) * \hat{b}(r, k) = \text{FFT} \left(\text{IFFT} [\hat{a}(r, k)] \text{IFFT} [\hat{b}(r, k)] \right).$$

Hence, in Fourier space, the PDE (3) is given by the large system of mN second-order complex equations

$$\hat{\mathbf{f}}(r, k) + \hat{\mathbf{U}}_{rr}(r, k) + \frac{1}{r} \hat{\mathbf{U}}_r(r, k) - \frac{k^2}{r^2} \hat{\mathbf{U}}(r, k) - i k \omega \hat{\mathbf{U}}(r, k) = 0,$$

for the N unknown Fourier coefficient vectors $\hat{\mathbf{U}}(r, k) \in \mathbb{C}^m$. Note that only derivatives with respect to the radial coordinate remain. Hence, we can express the PDE (3) as a system of

first-order ordinary differential equations (ODEs):

$$\begin{cases} \hat{\mathbf{U}}' &= \hat{\mathbf{U}}_r, \\ \hat{\mathbf{U}}'_r &= -\hat{\mathbf{f}} - \frac{1}{r} \hat{\mathbf{U}}_r + \frac{k^2}{r^2} \hat{\mathbf{U}} + i k \omega \hat{\mathbf{U}}, \\ r' &= 1, \end{cases} \quad (5)$$

where $'$ represents derivation with respect to r and the last equation renders the system autonomous. When split into real and imaginary parts, we now have $4mN + 1$ equations— $2m$ for each of the real and imaginary parts of the N Fourier modes—and $4mN + 1$ unknowns—the real and imaginary parts of the m -dimensional Fourier coefficient vectors $\hat{\mathbf{U}}(r, k)$, their m -dimensional derivatives $\hat{\mathbf{U}}_r(r, k)$, and ω . In practice, we only need to consider equations for the first $\frac{1}{2}N + 1$ modes, because $\mathbf{U}(r, \theta) \in \mathbb{R}^m$; the $\frac{1}{2}N - 1$ Fourier coefficient vectors $\hat{\mathbf{U}}(r, k)$ for the modes $k = \frac{1}{2}N + 1, \dots, N - 1$ are the complex conjugates of (non-zero) modes $k = 1, \dots, \frac{1}{2}N - 1$. Furthermore, $\hat{\mathbf{U}}(r, 0)$ and $\hat{\mathbf{U}}(r, \frac{1}{2}N)$ are real. Hence, we are interested in solutions to a system of $2mN + 1$ ODEs for $m(\frac{1}{2}N + 1)$ real and $m(\frac{1}{2}N - 1)$ imaginary parts of the Fourier coefficients and their derivatives, as well as the independent variable r .

The radial variable r is a time-like variable that fixes a particular solution segment for this system of ODEs. We consider $r \in [r_0, r_1]$, for some choices r_0 and r_1 . Together with $\theta \in [0, 2\pi)$, this defines an annulus as the spatial domain for the PDE (3). The spatial domain resembles a disk if r_0 is sufficiently small. If we were to let $r_1 \rightarrow \infty$, this would amount to a one-dimensional spatial dynamical system connecting the core at $r = 0$ to a far-field periodic travelling wave in the spirit of Woods & Champneys (1999). Moreover, computations of so-called boundary sinks, which connect the core to the far field, are useful when investigating spatiotemporal instabilities (Dodson & Sandstede, 2019).

To ensure that system (5) has a well-defined solution for each of the $\frac{1}{2}N + 1$ Fourier modes, we need to impose $2mN + 1$ boundary conditions and an additional phase-pinning condition. As suggested by Bordyugov & Engel (2007), we impose Neumann (zero radial derivative, or no flux) boundary conditions on \mathbf{U} on the inner and outer radial boundary of the chosen annulus in the spatial domain; in terms of the corresponding Fourier coefficients, these are

$$\begin{aligned} \hat{\mathbf{U}}'(r_0, k) &= 0, \\ \hat{\mathbf{U}}'(r_1, k) &= 0. \end{aligned} \quad (6)$$

To ensure uniqueness of the computed spiral wave, it is standard to impose a phase-pinning condition (Barkley, 1992). We use the suggestion from (Bordyugov & Engel, 2007) and fix the imaginary part of the first Fourier mode (or any other Fourier mode $k \geq 1$) of one of the variables at $r = r_1$:

$$\text{Im}(\hat{a}(r_1, 1)) = \text{constant}, \quad (7)$$

where we set this constant to 0. An alternative approach would be to replace this phase-pinning boundary condition with an integral condition. However, the described single boundary condition is qualitatively equivalent and computationally faster.

2.2 Starting point for continuation

The solution to the BVP (5)–(7) is an r -dependent family of Fourier coefficient vectors for the first $\frac{1}{2}N + 1$ modes. Using these Fourier coefficients and their complex-conjugates, we can reconstruct an approximation to the spiral wave defined on the annulus centred at the origin with radius $r \in [r_0, r_1]$ in the space-time domain. To obtain such a solution, we follow the continuation approach from (Bordyugov & Engel, 2007) that constructs the solution starting from an (almost) infinitely thin annulus. More precisely, while our goal is to find the spiral wave on a large disk, that is, with $r_0 = 0$ and very large r_1 , we start from a situation where $r_0 \approx r_1$ and allow r_0 and r_1 to vary, so that r_0 becomes very small and, subsequently, r_1 very large. This approach is useful, because the solution with $r_0 = r_1$ away from 0 can be approximated by a periodic travelling wave. Indeed, since the time periodicity of a (rigidly rotating) spiral wave is equivalent to a rotation in the (x, y) -plane, the solution restricted to the circle with radius $R = r_0 = r_1$ is, in fact, given by a periodic function of both space and time.

Periodic travelling waves can be found as periodic orbits of the one-dimensional travelling-frame equation

$$\mathbf{f}(\mathbf{U}) + \mathbf{U}_{\xi\xi} - \gamma \mathbf{U}_{\xi} = 0, \quad (8)$$

which is a stationary solution of the one-dimensional form of PDE (1) along the x -direction in absence of y , formulated with respect to the travelling-frame variable $\xi = x + \gamma t$ and the wavespeed γ of the periodic travelling wave. Such periodic travelling waves have wavelength L that depends on γ (Postlethwaite & Rucklidge, 2017). In (Postlethwaite & Rucklidge, 2017, 2019; Hasan et al., 2021), we investigated and computed such travelling waves, along with their stability properties, and showed that they, together with the limiting heteroclinic cycles for large wavelength values, provide a mechanism for the existence and stability of spiral waves of system (2).

Due to the spatiotemporal symmetry of a (rigidly rotating) spiral wave, a solution to equation (8) along a radial direction can equivalently be obtained as a solution along the angular direction, formulated in the co-rotating variable $\theta = \phi + \omega t$ as

$$\mathbf{f}(\mathbf{U}) + \frac{1}{R^2} \mathbf{U}_{\theta\theta} - \omega \mathbf{U}_{\theta} = 0, \quad (9)$$

where we assume that $r = R$ is constant. Since θ is an angular coordinate, it is natural to impose periodic boundary conditions

$$\mathbf{U}(2\pi) = \mathbf{U}(0) \quad \text{and} \quad \mathbf{U}_{\theta}(2\pi) = \mathbf{U}_{\theta}(0).$$

We remark that periodic solutions of (9) coincide with one-dimensional periodic orbits of (8) with wavespeed $\gamma = R\omega$ and wavelength $L = 2\pi R$.

Translated in terms of Fourier modes, we assume that $\widehat{\mathbf{U}}'(r, k) \approx 0$ and $\widehat{\mathbf{U}}''(r, k) \approx 0$ in system (5). In other words, the periodic solution of (9) is an approximate solution of

$$\widehat{\mathbf{f}}(k) - \frac{k^2}{R^2} \widehat{\mathbf{U}}(k) - i k \omega \widehat{\mathbf{U}}(k) = 0,$$

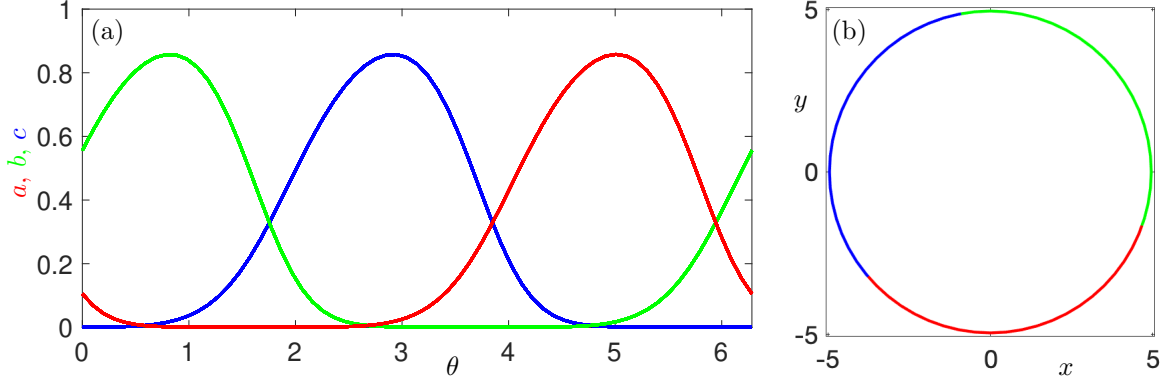


Figure 2: The first step for continuing spiral waves of system (2) with $\sigma = 3.2$, $\zeta = 0.8$, $\omega \approx 0.3346$ and radius $R = 5$. Panel (a) shows the θ -periodic solution for system (9) and panel (b) the corresponding distribution of the three populations a (red), b (green) and c (blue) given by system (5) and defined on a thin annulus in the (x, y) -plane of width $\varepsilon = 0.002$ centred around $r = R$.

defined on a very thin annulus with $r_1 = r_0 + \varepsilon$, for $0 < \varepsilon \ll 1$.

Figure 2 shows the starting solution for the BVP (5)–(7) with $\sigma = 3.2$ and $\zeta = 0.8$. Panel (a) shows the periodic solution of system (9) with period 2π for $R = 5$, which exists when $\omega \approx 0.3346$. This periodic solution is created in a Hopf bifurcation at $\omega \approx 0.2640$. Panel (b) shows the distribution of the one-dimensional periodic solution along a thin two-dimensional annulus; in Fourier space, this solution is given by approximately constant Fourier coefficient vectors for all $r \in [r_0, r_1]$. Here, we used $\varepsilon = 0.002$ and set

$$r_0 = R - \frac{1}{2}\varepsilon = 4.999 \quad \text{and} \quad r_1 = R + \frac{1}{2}\varepsilon = 5.001.$$

The red, green and blue regions represent the spatial dominance of a , b and c , respectively.

The spiral wave can now be found on a larger domain by continuation of this solution to the BVP (5)–(7), where we first decrease r_0 and then increase r_1 ; the resulting spiral wave for $r \in [0.01, 600]$ is shown in fig. 1. For the example system (2), where $m = 3$, this means the one-parameter continuation of a system of $2mN + 1 = 6N + 1$ real ODEs with the same number of unknowns. To obtain a good approximation to the spiral wave, it is imperative that a sufficiently large number N of Fourier modes is computed. The appropriate choice for N depends on the system. The almost two-fold reduction of the BVP, obtained by taking into account that real-valued solution vectors must have complex-conjugate pairs of Fourier coefficients, still leaves us with a very large system of equations. Since we wish to explore cases where the far-field dynamics limits onto the one-dimensional TW solution of (9), and since these solutions are associated with heteroclinic cycles, potentially with sharp transitions, one may need to work with many Fourier modes. Nevertheless, for the examples considered in this paper, we find that $N = 60$ is sufficient.

We note here that Barkley (1992) and Bär et al. (2003) constructed the initial solution by discretising the BVP into a large-scale system of Fourier-space ODEs (with 121×256 and 51×128 grid points, respectively) and integrating the ODEs until a spiral wave is obtained. This process is computationally expensive and requires a choice of parameters for which the existence of a spiral

wave is known *a priori*. In our study, we obtain the initial guess more reliably and efficiently by finding periodic orbits in a six-dimensional travelling-frame system of ODEs. Dodson & Sandstede (2019) solve the stationary problem for spiral waves using the MATLAB built-in function `fsolve` at each continuation step. In contrast, we perform all computations with the BVP set-up supported by the pseudo-arclength continuation software AUTO (Doedel, 1981; Doedel et al., 2007); this is also the approach taken by Bordyugov & Engel (2007).

The next steps in developing the method are to take advantage of the cyclic symmetry of this problem, and to address the issue of the boundary condition at the inner edge of the annulus, which needs to be changed once the inner radius r_0 approaches zero.

2.3 Exploiting cyclic symmetry

For systems of the form (1) satisfying Assumption 1.1, the cyclic symmetry of the nonlinear kinetic term provides an opportunity for further reduction of the number of Fourier coefficients that must be computed in the BVP (5)–(7) to obtain an N -mode approximation of a spiral wave solution. Indeed, the Fourier coefficients also have cyclic symmetry, because the Fourier transformation is an equivariant of this symmetry group. Note that the discretisation of the Fourier transform breaks this equivariance unless N is divisible by m . We explain how to implement the symmetry reduction for this restricted class of reaction-diffusion systems with the three-species model (2) as an example; hence, we assume that N is an integer multiple of $2m = 6$.

The cyclic symmetry of system (2), defined as the permutation $(a, b, c) \mapsto (b, c, a)$, introduces an additional phase-shift invariance of its spiral waves in the azimuthal direction, namely,

$$\begin{aligned} b(r, \theta) &= a(r, \theta - \frac{2\pi}{3}), \\ c(r, \theta) &= a(r, \theta + \frac{2\pi}{3}), \end{aligned}$$

for all r and θ . Hence, it is sufficient to consider only the first component of the co-rotating frame equation (3), which is given by

$$f_1 \left(a(r, \theta), a(r, \theta - \frac{2\pi}{3}), a(r, \theta + \frac{2\pi}{3}) \right) + a_{rr} + \frac{1}{r} a_r + \frac{1}{r^2} a_{\theta\theta} - \omega a_\theta = 0,$$

where f_1 is the first component of the kinetics function \mathbf{f} . This is related to the approach by (Wulff & Schebesch, 2006) to compute periodic orbits in ODEs with cyclic symmetry. The co-rotating frame equation in Fourier space for each mode k is then given by

$$\widehat{f}_1(r, k) + \widehat{a}_{rr}(r, k) + \frac{1}{r} \widehat{a}_r(r, k) - \frac{k^2}{r^2} \widehat{a}(k) - i k \omega \widehat{a}(r, k) = 0. \quad (10)$$

Here similarly, $\widehat{f}_1(r, k)$ is the k th coefficient of the discretised Fourier approximation of f_1 , which is the first component of the Fourier coefficient vector (4), given by

$$\widehat{a}(r, k) - [\widehat{a} * \widehat{a}](r, k) - (1 + \sigma + \zeta) [\widehat{a} * \widehat{b}](r, k) - (1 - \zeta) [\widehat{a} * \widehat{c}](r, k).$$

Since N is assumed to be divisible by $m = 3$, we can express $\widehat{b}(r, k)$ and $\widehat{c}(r, k)$ also in terms of

$\hat{a}(r, k)$, namely,

$$\hat{b}(r, k) = \hat{a}(r, k) e^{-2\pi i k / 3} \quad \text{and} \quad \hat{c}(r, k) = \hat{a}(r, k) e^{2\pi i k / 3}.$$

As a consequence, we now only need to solve $2N + 1$ real ODEs.

The boundary conditions for the reduced BVP are just the first components of each of the two conditions in (6), with the same phase-pinning condition (7). Hence, they are given by

$$\begin{aligned} \hat{a}'(r_0, k) &= 0, \\ \hat{a}'(r_1, k) &= 0, \\ \text{Im}(\hat{a}(r_1, 1)) &= 0. \end{aligned} \tag{11}$$

In general, for a system with m species, the number of real differential equations is reduced by almost a factor m , from $2mN + 1$ to $2N + 1$. In other words, the increase in the number of species m in system (1) has no effect on the size of the BVP and only adds a minor extra cost to the computation because of the additional convolutions in the first component of the Fourier coefficient vector $\hat{\mathbf{f}}$. We note here also that a similar reduction can be obtained when computing spiral waves that obey a different permutation symmetry, involving a subset of the m species, but the efficiency gains in such instances will be smaller than a factor m .

2.4 Growing the spiral wave solution by continuation

We use the substantially reduced BVP (10)–(11) to compute a spiral wave for system (2) with $\sigma = 3.2$ and $\zeta = 0.8$. Recall that we already found a starting solution for these parameter values in the form of a periodic travelling wave interpreted as a solution on a very thin annulus with inner radius $r_0 = 4.999$ and outer radius $r_1 = 5.001$; see fig. 2. We set $N = 60$ and initialise the continuation with the Fourier coefficients corresponding to this travelling wave solution. We then continue the BVP (10)–(11) in the direction of decreasing r_0 while keeping r_1 fixed and treating the angular frequency ω as a free parameter. Figure 3 shows four snapshots of this continuation process, where we plot the solution in the (x, y) -plane with $r_0 = 3$ in panel (a), $r_0 = 1$ in panel (b), $r_0 = 0.5$ in panel (c), and $r_0 = 0.01$ in panel (d), which is the last step after which we stopped the continuation. Panel (d) illustrates that the computed solution can be viewed as a computation on a disk of radius $r_1 = 5.001$ in the (x, y) -plane, even though the domain is, in reality, an annulus, and the inner boundary condition needs to be considered before r_0 can be decreased further. It is also clear that r_1 is too small to show the true nature of the spiral wave.

The size of the annular spatial domain can be increased with a second continuation step where we keep r_0 fixed and increase r_1 to obtain a spiral wave solution on a sufficiently large domain. Figure 4 shows the evolution of the spiral wave as r_1 is increased. As in fig. 3, we show each stage of the continuation step by plotting the spiral wave in the (x, y) -plane at a fixed moment in time; here, $r_1 = 30$ in panel (a), $r_1 = 55$ in panel (b), $r_1 = 85$ in panel (c), and $r_1 = 110$ in panel (d). Panel (e) illustrates how the angular frequency ω varies during the continuation; here, we plot ω versus the outer radius r_1 . Note that the initial value $\omega \approx 0.3346$ for $[r_0, r_1] = [4.999, 5.001]$ has increased to $\omega \approx 0.5537$ as r_0 was decreased to 0.01. As the outer radius of the spiral is increased

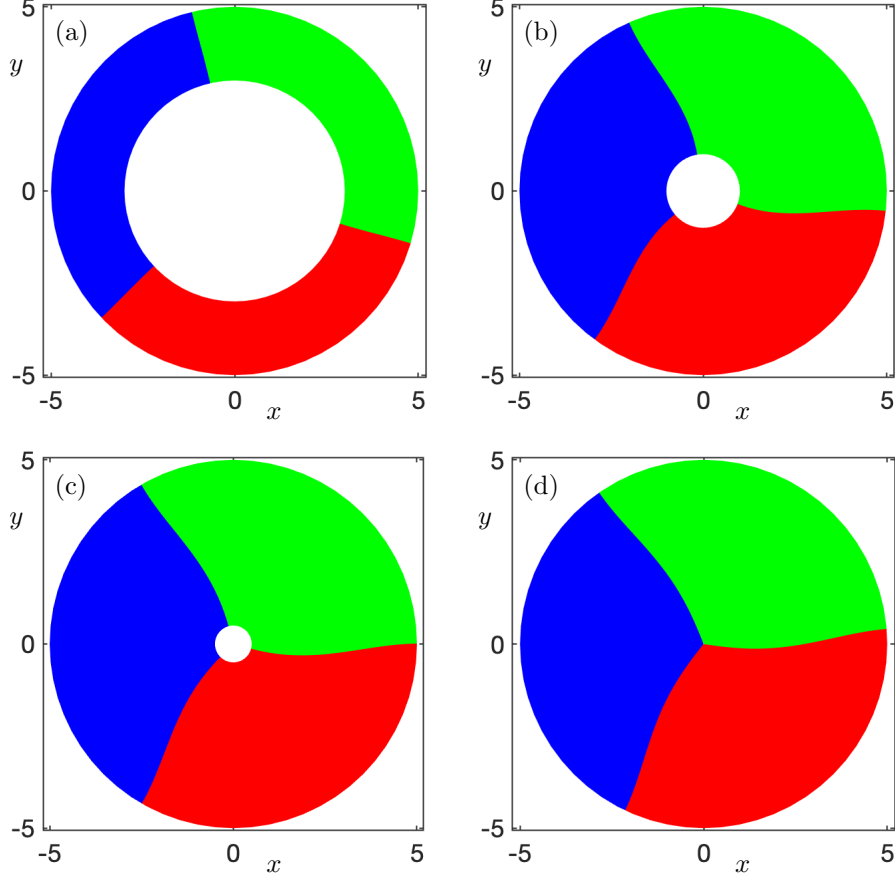


Figure 3: Illustration of the continuation steps taken to compute a spiral wave for system (2) with $\sigma = 3.2$ and $\zeta = 0.8$ by varying the inner radius r_0 . Starting from the solution shown in fig. 2(b) with $N = 60$, panels (a)–(d) show the solutions to the BVP (10)–(11) on the (x, y) -plane at a fixed moment in time, where $r_0 = 3$, $r_0 = 1$, $r_0 = 0.5$, and $r_0 = 0.01$, respectively.

from $r_1 = 5.001$, the angular frequency ω drops again sharply, and then levels off very quickly to $\omega \approx 0.4400$. We stopped the continuation when $r_1 = 600$; the spiral wave for this value is shown in fig. 1(a) and $\omega \approx 0.4400$ here as well.

2.5 Boundary conditions at the core: spiral waves on a full disk

In the initial thin annulus, we used Neumann boundary conditions in the radial direction in order to have an initial solution that is approximately independent of r . As the inner radius r_0 is decreased towards zero, these boundary conditions are no longer appropriate since they lead to singularities in the Laplacian. To see this, consider one Fourier coefficient $\hat{a}(r, k)$ with wavenumber k ; for small r , this coefficient will behave as

$$\hat{a}(r, k) \sim r^j e^{ik\phi},$$

where $j \geq 0$ is an integer. The corresponding Laplacian is

$$\nabla^2 r^j e^{ik\phi} = (j^2 - k^2) r^{j-2} e^{ik\phi}.$$

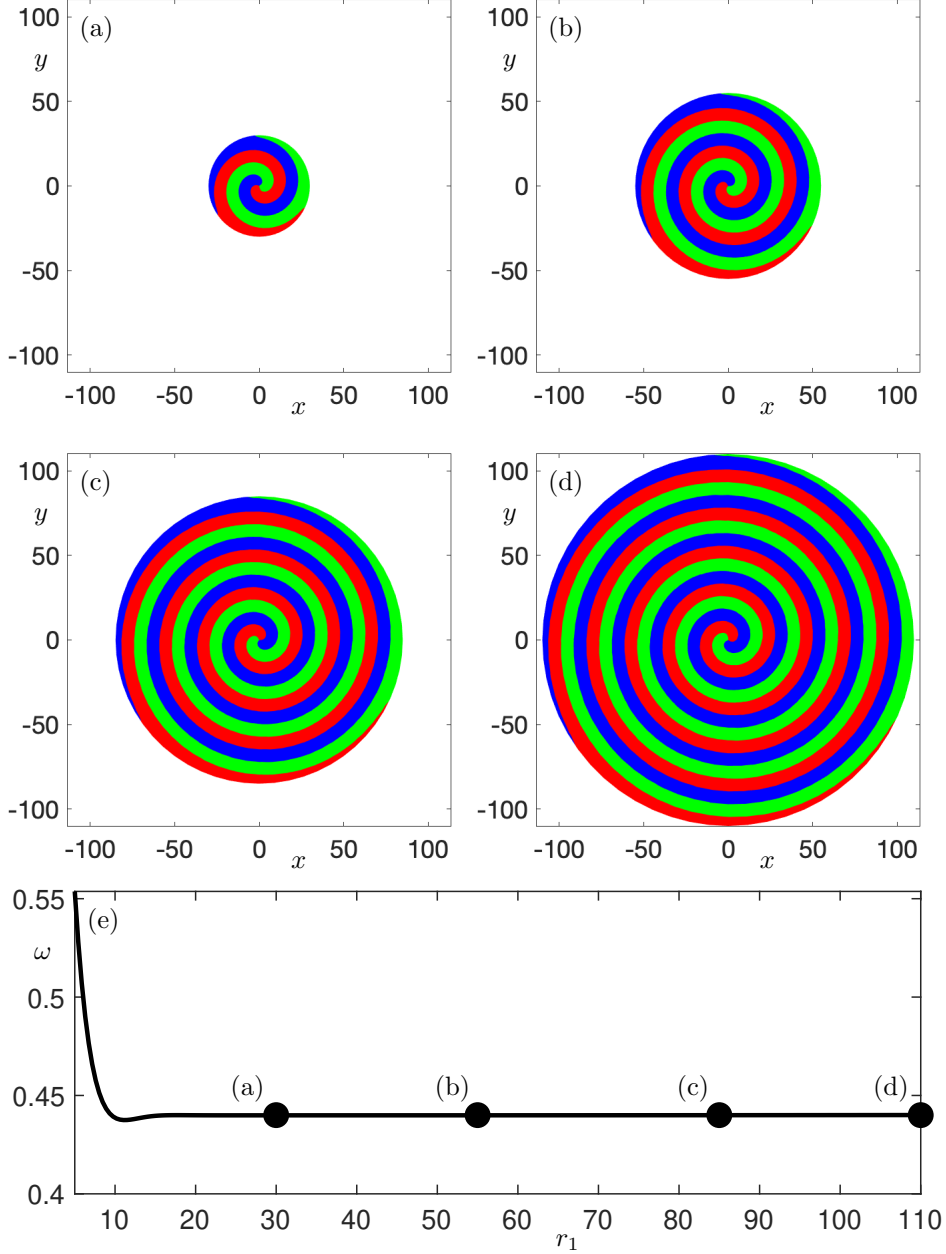


Figure 4: Illustration of the continuation steps taken to compute a spiral wave for system (2) with $\sigma = 3.2$, $\zeta = 0.8$ and $r_0 = 0.01$ by varying the outer radius r_1 . Starting from the solution shown in fig. 3(d) with $N = 60$, panels (a)–(d) show the solutions to the BVP (10)–(11) on the (x, y) -plane at a fixed moment in time, where $r_1 = 30$, $r_1 = 55$, $r_1 = 85$, and $r_1 = 110$, respectively. Panel (e) shows the angular frequency ω versus r_1 .

The Laplacian of $\hat{a}(r, k)$ should be well behaved at any point on the disk, so at $r = 0$, we must have either $j^2 - k^2 = 0$ or $j \geq 2$. Therefore, for the zeroth Fourier mode ($k = 0$), we have $j = 0$ or $j \geq 2$, that is, the radial derivative of the zeroth mode is zero at $r = 0$. For the first Fourier mode ($k = 1$), we can have $j = 1$ or $j \geq 2$, so the first Fourier mode is zero at $r = 0$. Similarly, for $k \geq 2$, we must have $j \geq 2$. Imposing Neumann boundary conditions (6), where $\hat{\mathbf{U}}'(r_0, k) = 0$ for all k , allows for the possibility that $\hat{a}(0, k) \neq 0$ for all k , which leads to an infinite Laplacian for $k \geq 1$ in the limit $r_0 \rightarrow 0$. Hence, in order to continue to $r_0 = 0$ without a singularity in

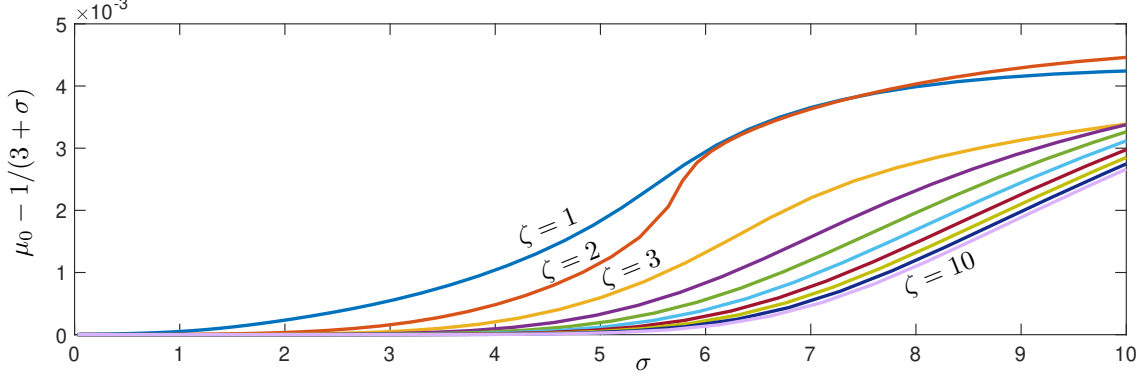


Figure 5: Dependence on the parameter σ of the value $a = b = c = \mu_0$ at the core of the spiral wave for system (2) computed with radius $R = 30$ and $N = 60$ Fourier modes using Dirichlet and Neumann boundary conditions (12). Shown are results from numerical continuation with respect to σ for fixed $\zeta = 1, 2, \dots, 10$. The curves illustrate the difference $\mu_0 - \frac{1}{3+\sigma}$ for each of the ten different values of ζ .

the Laplacian, we require a Neumann boundary condition only for $k = 0$ and impose Dirichlet boundary conditions at $r = r_0$ for all other k :

$$\begin{aligned}\widehat{\mathbf{U}}'(r_0, 0) &= 0, \\ \widehat{\mathbf{U}}(r_0, k) &= 0, \text{ for } k > 0.\end{aligned}\tag{12}$$

As $r_0 \rightarrow 0$, the cyclic symmetry implies that a , b and c all take on the same value at $r = 0$: we denote this common value by μ_0 . Note that these boundary conditions translate to a Dirichlet boundary condition in physical space, namely, $\mathbf{U}(0, \theta) = \mu_0$. These boundary conditions must be coupled with the phase condition (7).

As was the case for the Neumann boundary conditions (6), the modified Dirichlet boundary conditions (12) are also readily implemented for the reduced BVP (10)–(11), because they translate directly to conditions for the component \widehat{a} of $\widehat{\mathbf{U}}$ only. Rather than set up the modified BVP from scratch (which would not work in the initial thin annulus), we continue the spiral wave that was already computed as a solution to BVP (10)–(11) with Neumann boundary conditions to that of a BVP with the modified Dirichlet boundary conditions via a homotopy step. We define, for $k > 0$, the hybrid boundary conditions

$$(1 - \lambda) \widehat{\mathbf{U}}'(r_0, k) + \lambda \widehat{\mathbf{U}}(r_0, k) = 0,$$

where we initially set $\lambda = 0$. We then continue the known solution from $\lambda = 0$ to $\lambda = 1$, while keeping ω as a free parameter. Following this, we can continue r_0 to zero resulting in a spiral wave on a full disk with radius $R = r_1$.

3 Comparison of computational results

To test the accuracy and efficiency of our modified method, we compare the results obtained from the reduced BVP (10)–(11) with direct simulations of the laboratory-frame PDEs (2). We note

that the full BVP (5)–(7) produces solutions with the same cyclic symmetry as assumed in the reduced BVP (10)–(11), so the results are identical, with a substantial gain in efficiency.

For the BVP method, we compute spiral waves on a disk with radius $R = 30$ and continue them with respect to ω , σ and ζ . The PDE simulations were conducted on a large square box in the (x, y) -plane of size 2000×2000 ; see (Postlethwaite & Rucklidge, 2017; Hasan et al., 2021) for precise details on this computational set-up.

3.1 Values of a , b and c at the core

We have defined μ_0 to be the common value of a , b and c at the core $r = 0$. Results from direct PDE simulation show that this common value is close to (but not equal to) the coexistence equilibrium point value, $a = b = c = \frac{1}{3+\sigma}$ (Szczesny et al., 2014; Postlethwaite & Rucklidge, 2017). Our continuation scheme gives the same result for the values of a , b and c at the core as the direct simulation of the PDEs. In fig. 5 we compare μ_0 to $\frac{1}{3+\sigma}$. The continuation results reveal that $\mu_0 \rightarrow \frac{1}{3+\sigma}$ as $\sigma \rightarrow 0$, and more quickly for smaller ζ . Even for larger σ , the difference is only of order 10^{-3} . We note that this comparison is not possible without the final step of changing the boundary conditions and continuing to $r_0 = 0$.

3.2 Angular frequency of spiral waves

Postlethwaite & Rucklidge (2017) conjectured that the angular frequency of the spiral waves was related to the imaginary part of the complex eigenvalue at the coexistence equilibrium point. In particular, they suggested a linear relationship

$$\omega \sim \frac{2}{3} \times \frac{\sqrt{3}(\sigma + 2\zeta)}{2(3 + \sigma)}, \quad (13)$$

where the $\frac{2}{3}$ pre-factor was obtained by fitting a straight line to PDE simulations in the range $0.1 \leq \sigma \leq 20$ and $0 \leq \zeta \leq 10$. The spiral angular frequency in the simulations was only estimated at parameter values where reasonably large stable spirals could be found.

To test this conjecture, we computed the angular frequency ω by continuation. Figure 6 shows the relation between the angular frequency ω and system parameters σ and ζ . Panel (a) shows this relation in the (ζ, ω) -plane for $\sigma = 1, 2, \dots, 10$. By inspection, we find that all curves are almost linear with an approximate slope of $\sqrt{3}(3 + \sigma)^{-1}$ rather than the conjectured $\frac{2}{3}\sqrt{3}(3 + \sigma)^{-1}$ as postulated by Postlethwaite & Rucklidge (2017). This is more evident in panel (b) where we plot the same curves with ω rescaled by a factor of $\sqrt{3}(3 + \sigma)^{-1}$; note that the slopes are all about 1 in this projection.

Figure 6(c) shows the same curves with $2\omega(3 + \sigma)/\sqrt{3}$ plotted against $2\zeta + \sigma$. Our continuation results, over a full range of σ and ζ (each between 1 and 10) contradict the conjecture of Postlethwaite & Rucklidge (2017). The observations of Postlethwaite & Rucklidge (2017) were predominantly based on relatively small values of σ and ζ , where large enough stable spirals could be found and their frequencies measured. There is a rough agreement for small σ and ζ , but the discrepancies for larger values are quite significant; see (Postlethwaite & Rucklidge, 2017, fig. 4).

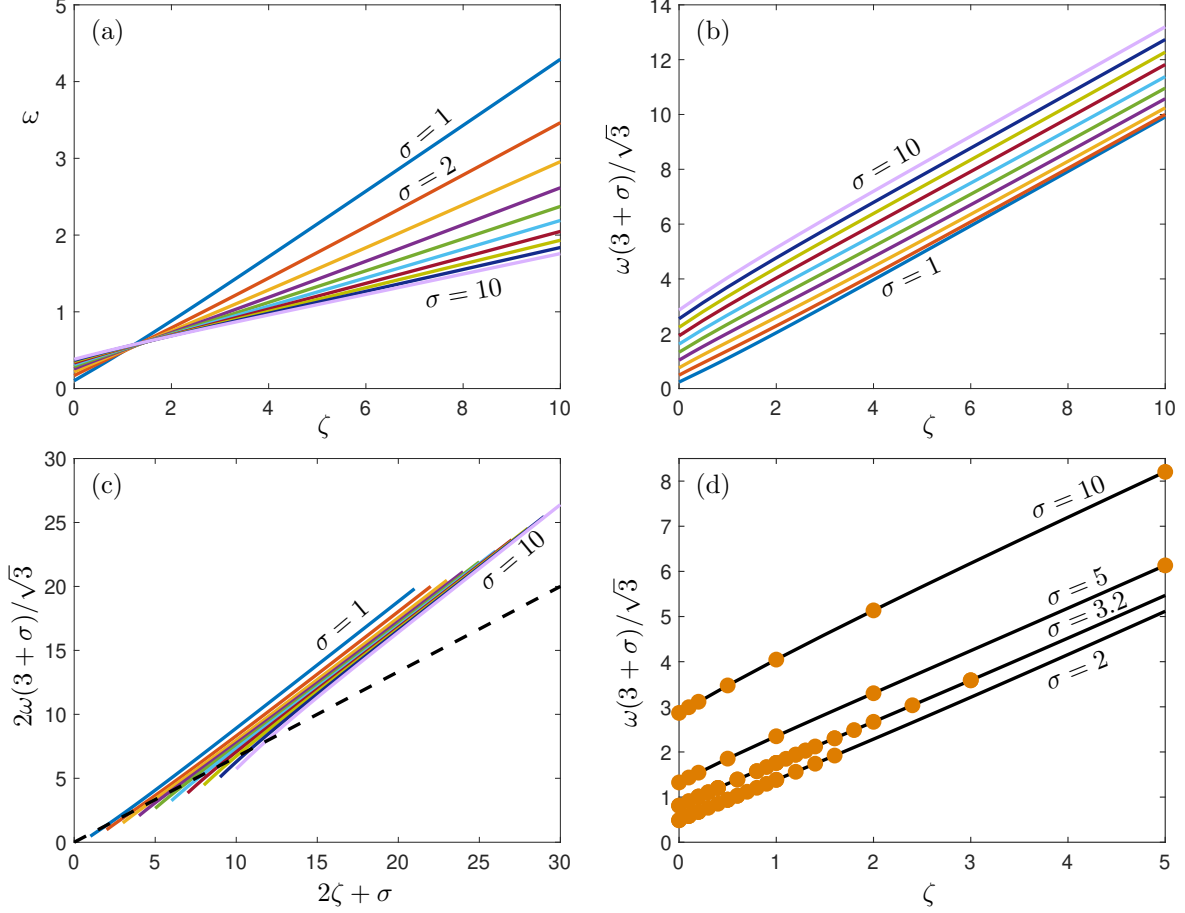


Figure 6: Dependence of the angular frequency ω on parameters ζ and σ for spiral waves of system (2) computed on a disk with radius $R = 30$ and $N = 60$ Fourier modes. Panels (a)–(c) show the curves for fixed $\sigma = 1, 2, \dots, 10$ in three different projections. Panel (d) shows a comparison between the continuation results (black curves) and direct simulations of the laboratory-frame equations (2) (orange dots) for $\sigma = 2, 3.2, 5.0$ and 10.0 .

Figure 6(d) demonstrates that the continuation results (black curves) and direct simulations (orange dots) agree extremely well.

We find that the angular frequency is better approximated by the linear function

$$\omega \approx \frac{\sqrt{3}(\frac{3}{2}\sigma + 2\zeta)}{2(3 + \sigma)};$$

compare with (13). While this value is still similar to the imaginary part of the coexistence equilibrium, the difference is not just a factor of $\frac{2}{3}$. On the other hand, our updated value still indicates linear dependency on ζ and the slope $\sqrt{3}(3 + \sigma)^{-1}$ appears to be valid over a large range of values for both σ and ζ .

4 Five-species model

In this section, we illustrate the gains in computational efficiency obtained when taking into account the cyclic symmetry of spiral waves in larger heteroclinic networks. Heteroclinic networks

Equilibrium	ξ_1	ξ_2	ξ_3	ξ_4	ξ_5
(a, b, c, p, q)	$(1, 0, 0, 0, 0)$	$(0, 1, 0, 0, 0)$	$(0, 0, 1, 0, 0)$	$(0, 0, 0, 1, 0)$	$(0, 0, 0, 0, 1)$
Equilibrium	η_1	η_2	η_3	η_4	η_5
(a, b, c, p, q)	$(s, s, 0, 0, s)$	$(s, s, s, 0, 0)$	$(0, s, s, s, 0)$	$(0, 0, s, s, s)$	$(s, 0, 0, s, s)$

Table 1: Equilibrium points in the heteroclinic network of system (14), where $s = (3 + \sigma)^{-1}$.

of five competing species in an ODE form was first studied by Field & Richardson (1992) and then further investigated in Podvigina (2013), Afraimovich et al. (2016) and Bayliss et al. (2020). Just as for the three-strategy Rock–Paper–Scissors game, the extended game of Rock–Paper–Scissors–Lizard–Spock (Kass & Bryla, 1995) can be viewed as a population model for competing species; each population density represents the probability density of winning the game when consistently playing the same strategy, e.g., always Rock, or always Scissors. Hence, the game can be modelled as a PDE of the form (1) using similar equations as in system (2), but with $m = 5$ species. More precisely, we consider

$$\begin{cases} \dot{a} &= a(1 - \rho - (\sigma + \zeta)(b + p) + \zeta(c + q)) + \nabla^2 a, \\ \dot{b} &= b(1 - \rho - (\sigma + \zeta)(c + q) + \zeta(p + a)) + \nabla^2 b, \\ \dot{c} &= c(1 - \rho - (\sigma + \zeta)(p + a) + \zeta(q + b)) + \nabla^2 c, \\ \dot{p} &= p(1 - \rho - (\sigma + \zeta)(q + b) + \zeta(a + c)) + \nabla^2 p, \\ \dot{q} &= q(1 - \rho - (\sigma + \zeta)(a + c) + \zeta(b + p)) + \nabla^2 q, \end{cases} \quad (14)$$

where $p(t, x, y)$ and $q(t, x, y)$ are two additional (non-dimensionalised) species and $\rho = a + b + c + p + q$. Here, we assume that the removal rate σ and replacement rate ζ are the same for all species interactions. Spatiotemporal patterns for five-species reaction-diffusion systems have been obtained via stochastic simulations and studied in (Hawick, 2011; Cheng et al., 2014; Park et al., 2017), but a precise continuation or computation of the spiral wave has not been attempted before.

System (14) has five equilibria at which only one population (a , b , c , p , and q , respectively) survives, which we denote by ξ_i , where the index $i = 1, 2, 3, 4, 5$ represents the component in the vector (a, b, c, p, q) of the surviving species. There are also five equilibria $\eta_1 - \eta_5$, each of which has three surviving populations; more precisely, at each equilibrium η_i , components with indices $i - 1, i, i + 1 \pmod{5}$ survive. The coordinates of the equilibrium points $\xi_1 - \xi_5$ and $\eta_1 - \eta_5$ are given in table 1. Note that each triple $\xi_{i-1}, \xi_i, \xi_{i+1}$ lies in an invariant subspace that contains the equilibrium η_i . Moreover, there exists a coexistence equilibrium with $a = b = c = p = q = 1/(5 + 2\sigma)$, where all five species coexist.

Figure 7 shows all possible five-component heteroclinic cycles of system (14) in the form of a directed graph, where each node represents an equilibrium and the edges the connecting orbits. As for the three-species model, there exists a heteroclinic cycle that consecutively connects all five equilibria ξ_i with $i = 1, \dots, 5$; this cycle is highlighted in red in fig. 7(a) and we refer to it as Γ_1 . There exists a second heteroclinic cycle between these five equilibria: instead of connecting ξ_i to ξ_{i+1} for $i = 1, \dots, 5 \pmod{5}$, the connection is from ξ_i to ξ_{i+3} for $i = 1, \dots, 5 \pmod{5}$; this cycle is highlighted in blue in fig. 7(a) and we refer to it as Γ_2 . There also exists a heteroclinic

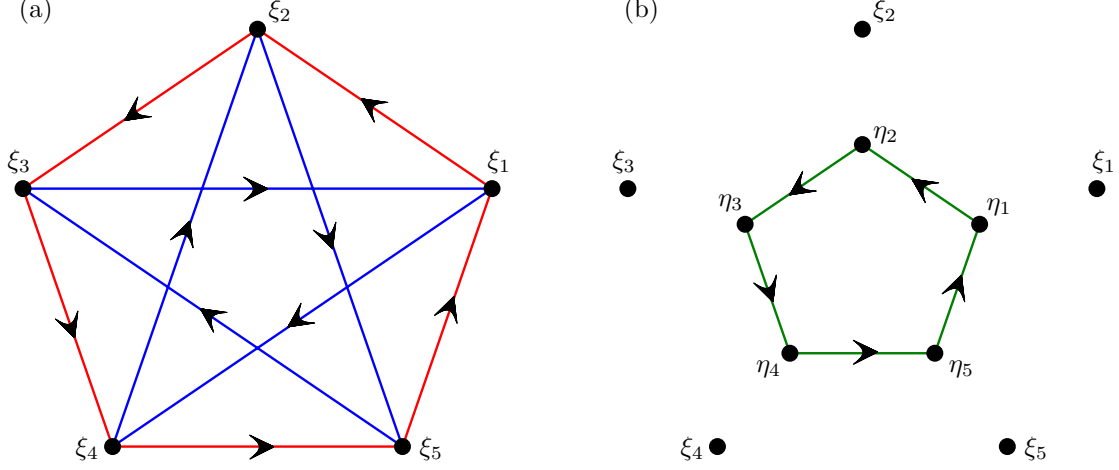


Figure 7: Heteroclinic network of system (14) with nodes $\xi_1, \xi_2, \xi_3, \xi_4$ and ξ_5 that represent equilibria at which only one population survives, and $\eta_1, \eta_2, \eta_3, \eta_4$ and η_5 that represent equilibria at which three populations survive. Panel (a) highlights heteroclinic cycles Γ_1 (red) and Γ_2 (blue) involving all five equilibria ξ_i , and panel (b) shows the heteroclinic cycle Γ_3 (green) involving all five equilibria η_i , with $i = 1, \dots, 5$; see table 1 for the definition of the equilibria.

cycle between the other five equilibria, connecting η_i to η_{i+1} for $i = 1, \dots, 5 \pmod{5}$; this cycle is highlighted in green in fig. 7(b) and we refer to it as Γ_3 .

There are many other heteroclinic cycles, some longer and some involving fewer than five equilibria. For example, there exist five heteroclinic cycles in system (14) between three of the five equilibria ξ_i with $i = 1, \dots, 5$. More precisely, these are formed by triples $\xi_{i-1}, \xi_i, \xi_{i+1}$ that surround an associated coexistence equilibrium η_i , with $i = 1, \dots, 5 \pmod{5}$. Hence, the dynamics is entirely restricted to the lower-dimensional invariant subspace involving these equilibria, which is perfectly described by system (2). Here, we focus only on the dynamics of the heteroclinic cycles between five equilibria.

With our reduced BVP method, we take advantage of the cyclic symmetry in the system; in complete analogy to the steps outlined in section 2.3, we can express each of the five species in terms of appropriate phase shifts of the first. As a starting solution, we determine the associated periodic travelling wave given as a periodic orbit of the one-dimensional travelling-frame equation

$$\mathbf{f}(\mathbf{U}) + \mathbf{U}_{\xi\xi} - \gamma \mathbf{U}_{\xi} = 0, \quad (15)$$

where the solution vector $\mathbf{U}(\xi) = [a(\xi), b(\xi), c(\xi), p(\xi), q(\xi)]^T \in \mathbb{R}^m$ now represents $m = 5$ species, the vector \mathbf{f} represents the kinetics terms in system (14), and $\xi = x + \gamma t$ is the travelling-frame variable. In the travelling-frame coordinate, we find periodic orbits that are associated to only two of the three heteroclinic cycles between five equilibria, namely, Γ_2 and Γ_3 , that is, the blue and green cycles highlighted in fig. 7. Using these two periodic orbits, we set up two different versions of the reduced BVP (10)–(11): for cycle Γ_2 , we can exploit the permutation symmetry

$$(a, b, c, p, q) \mapsto (p, q, a, b, c),$$

and for cycle Γ_3 , we use

$$(a, b, c, p, q) \mapsto (b, c, p, q, a).$$

Therefore, the first component of the co-rotating frame equation (3) for cycle Γ_2 is given by

$$f_1 \left(a(r, \theta), a(r, \theta - \frac{4\pi}{5}), a(r, \theta + \frac{2\pi}{5}), a(r, \theta - \frac{2\pi}{5}), a(r, \theta + \frac{4\pi}{5}) \right) + \\ a_{rr} + \frac{1}{r} a_r + \frac{1}{r^2} a_{\theta\theta} - \omega a_\theta = 0,$$

where

$$f_1(a, b, c, p, q) = a(1 - \rho - (\sigma + \zeta)(b + p) + \zeta(c + q)).$$

Similarly, for cycle Γ_3 , we use

$$f_1 \left(a(r, \theta), a(r, \theta - \frac{2\pi}{5}), a(r, \theta - \frac{4\pi}{5}), a(r, \theta + \frac{4\pi}{5}), a(r, \theta + \frac{2\pi}{5}) \right) + \\ a_{rr} + \frac{1}{r} a_r + \frac{1}{r^2} a_{\theta\theta} - \omega a_\theta = 0.$$

In this way, we reduce the number of real differential equations from $2mN + 1 = 10N + 1$ to $2N + 1$, which is about a five-fold reduction.

The numerical continuation is performed in Fourier space, using equation (10) for each of the first $\frac{1}{2}N + 1$ Fourier modes. The k th coefficient of the discretised Fourier approximation of f_1 is now given by

$$\hat{f}_1(r, k) = \hat{a} - \hat{a} * \hat{a} - (1 + \sigma + \zeta) \hat{a} * (\hat{b} + \hat{p}) - (1 - \zeta) \hat{a} * (\hat{c} + \hat{q}), \quad (16)$$

where we dropped the dependence on (r, k) for notational convenience.

The modifications of the set-up for the BVP (10)–(11) are all that is needed to compute spiral waves of system (14). Note that it hardly matters that there are now five rather than three species, because we still only compute the evolution of the population density of one of these species; the number of differential equations and boundary conditions are the same for both the three-species and five-species models. The only difference in computational cost is the evaluation of five instead of three nonlinear terms.

We compute the spiral waves of system (14) that correspond to the two cycles Γ_2 and Γ_3 on a full disk in the (x, y) -plane, centred at the origin, with inner radius $r_0 = 0$ and outer radius $r_1 = 300$, by solving the BVP(10)–(11) with Dirichlet boundary conditions (12). The result is shown in fig. 8, where the colours red, green, blue, yellow, and black represent the populations a , b , c , p , and q , respectively. In the top row, we show the spiral wave in the (x, y) -plane with colours indicating the species that is dominant in that region. The bottom row shows the spatial profile along the outermost circle of the computed domain (at $r = 300$); here the horizontal axis is the 2π -periodic co-rotating variable θ . Panels (a1) and (a2) are for the spiral wave associated with the cycle Γ_2 and panels (b1) and (b2) for the spiral wave associated with Γ_3 . Note that the profile shown in panel (a2) lies close to the heteroclinic cycle Γ_2 . Similarly, the profile shown in panel (b2) is reminiscent of the heteroclinic cycle Γ_3 ; the small oscillations around $\frac{1}{3+\sigma}$ are

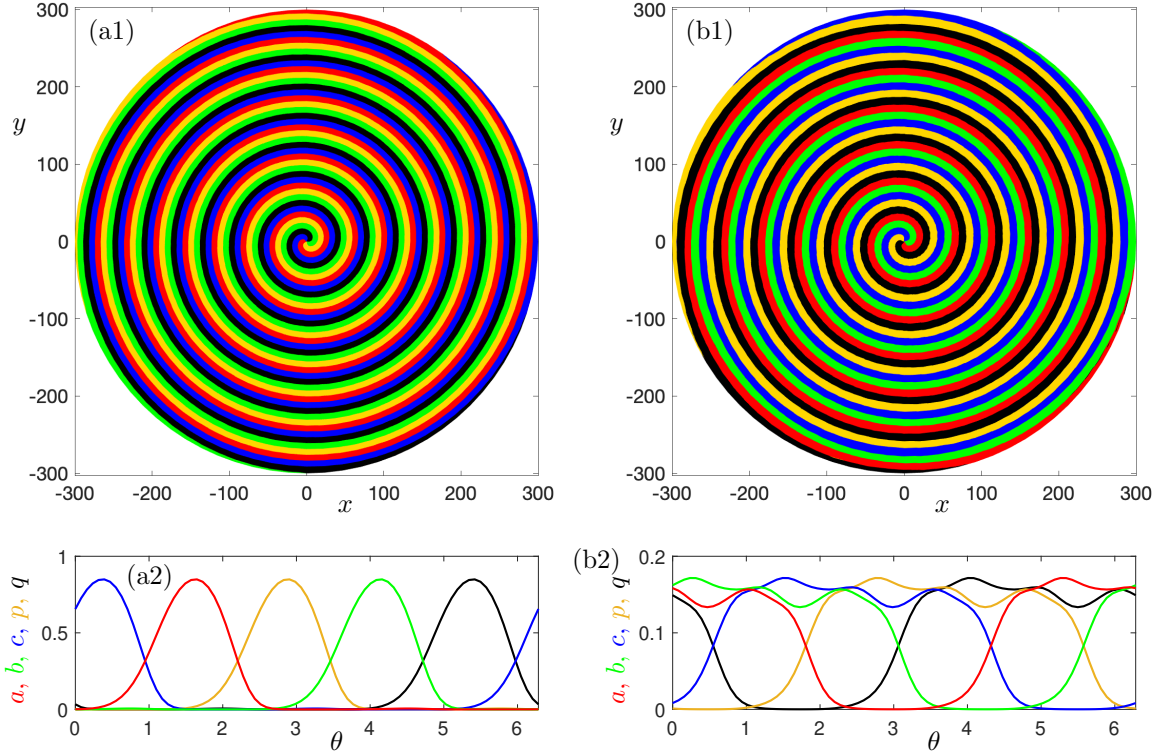


Figure 8: Spiral waves of the five-species system (14) with $\sigma = 3.2$, $\zeta = 0.8$ computed on a full disk of radius $R = 300$ with $N = 80$ Fourier modes. Panels (a1) and (b1) show the spiral waves that correspond to cycles Γ_2 and Γ_3 with angular velocities $\omega \approx 0.260376$ and $\omega \approx 0.093288$, respectively; panels (a2) and (b2) show the corresponding distribution of the five species along outer boundary of the domain.

formed due to the saddle-focus nature of the equilibria $\eta_1 - \eta_5$. The core of both spiral waves shown in fig. 8 admits a common value for all five species. This value is close to the coexistence equilibrium $a = b = c = p = q = 1/(5 + 2\sigma)$, for both spirals, within 10^{-3} .

5 Discussion

This paper presents a numerical study of spiral waves in systems of symmetric heteroclinic networks. As an adaptation of the method introduced by Bordyugov & Engel (2007), we combined methods from discrete Fourier transforms, boundary-value problem formulations and group symmetries to generate a fast algorithm for computing and continuing spiral waves in cyclic dominance models. The proposed continuation method is an efficient way to explore the dynamics of spiral waves in symmetric systems. In particular, this method is an efficient way to explore spiral waves in a large heteroclinic networks of five (or more) competing species. We emphasise that the numerical method presented here can be modified to compute spiral waves for any reaction-diffusion system. More precisely, one needs to follow the steps presented in section 2 but ignore the symmetry exploitation presented in section 2.3.

We found that the angular frequency of spiral waves in system (2) was not directly related to the linear frequency of the equilibrium point at the core, as postulated by Postlethwaite & Rucklidge

(2017). The results from the modified continuation method also accurately match results from direct integration. We introduced Dirichlet boundary conditions (12) in order to obtain a bounded (non-singular) Laplacian term at the core as $r \rightarrow 0$. Applying these boundary conditions allow us to compute spiral waves on a full disk instead of an annulus. What is more, a challenging task in direct simulations is to locate and determine the common value of the variables at the core. Using our boundary conditions, we are able to determine the precise location and value at the core and investigate its dynamics.

Spatiotemporal instabilities of spiral waves come in different shapes and forms and may emerge from the far field, the core, or the boundary conditions (Dodson & Sandstede, 2019; Sandstede & Scheel, 2000, 2020). The Dirichlet boundary conditions (12) proposed in this paper is an essential starting point to compute and identify core instabilities. Just as we have done for travelling waves (Hasan et al., 2021), we plan to compute spectra of heteroclinic-induced spiral waves. Such computations require a coupling of the stationary problem and the augmented eigenvalue problem. Hence, obtaining linear spectra of spiral waves in large domains is a computationally expensive task. Our symmetry-based reduction can be applied to reduce the number of ODEs for the augmented eigenvalue problem and thus facilitate fast and efficient computation of spectra of spiral waves in spatiotemporal systems of large heteroclinic networks. One shortcoming of this approach is that the augmented eigenvalue problem would have full rank, which makes the stability analysis computationally expensive. However, one can perform iterative steps to compute the largest eigenvalue or even a selected number of dominant eigenvalues efficiently (Dijkstra et al., 2014; Saad, 2011).

For the five-species system, we were only able to find spiral waves associated with two of the three heteroclinic cycles between five equilibria. At first glance, it may seem like the heteroclinic cycles Γ_1 and Γ_2 are of a similar type, but the heteroclinic connections in Γ_1 are two dimensional, and the heteroclinic connections in Γ_2 are one dimensional—more precisely, there exists a two-dimensional manifold of connecting orbits between ξ_1 and ξ_2 . It may be that this structural difference has a role to play in the bifurcation of long-period periodic orbits from these heteroclinic cycles. We plan to investigate this in future work by examining system (14) with one spatial dimension in the travelling frame coordinates and investigating the heteroclinic bifurcations which occur in the resulting 10-dimensional system of ODEs.

Acknowledgment

We are grateful for discussions with Andrus Giraldo, Chris Marcotte, Mauro Mobilia and Stephanie Dodson.

Funding

University of Auckland (FRDF-3714924 to C.R.H., H.M.O. & C.M.P.); Royal Society Te Apārangi, New Zealand (17-UOA-096 to C.M.P.); London Mathematical Laboratory; Leverhulme Trust (RF-2018-449/9 to A.M.R.).

References

- Afraimovich, V. S., Moses, G. & Young, T. (2016) Two-dimensional heteroclinic attractor in the generalized Lotka–Volterra system. *Nonlinearity*, **29**(5), 1645.
- Bär, M., Bangia, A. K. & Kevrekidis, I. G. (2003) Bifurcation and stability analysis of rotating chemical spirals in circular domains: Boundary-induced meandering and stabilization. *Physical Review E*, **67**(5), 056126.
- Barkley, D. (1992) Linear stability analysis of rotating spiral waves in excitable media. *Physical Review Letters*, **68**(13), 2090.
- Bayliss, A., Nepomnyashchy, A. & Volpert, V. (2020) Beyond rock-paper-scissors systems—Deterministic models of cyclic ecological systems with more than three species. *Physica D: Nonlinear Phenomena*, **411**, 132585.
- Bordyugov, G. & Engel, H. (2007) Continuation of spiral waves. *Physica D: Nonlinear Phenomena*, **228**(1), 49–58.
- Cheng, H., Yao, N., Huang, Z.-G., Park, J., Do, Y. & Lai, Y.-C. (2014) Mesoscopic interactions and species coexistence in evolutionary game dynamics of cyclic competitions. *Scientific reports*, **4**(1), 1–7.
- Dijkstra, H. A., Wubs, F. W., Cliffe, A. K., Doedel, E., Dragomirescu, I. F., Eckhardt, B., Gelfgat, A. Y., Hazel, A. L., Lucarini, V., Salinger, A. G., Phipps, E. T., Sanchez-Umbria, J., Schuttelaars, H., Tuckerman, L. S. & Thiele, U. (2014) Numerical bifurcation methods and their application to fluid dynamics: analysis beyond simulation. *Communications in Computational Physics*, **15**(1), 1–45.
- Dodson, S. & Sandstede, B. (2019) Determining the source of period-doubling instabilities in spiral waves. *SIAM Journal on Applied Dynamical Systems*, **18**(4), 2202–2226.
- Doedel, E. J. (1981) AUTO: A program for the automatic bifurcation analysis of autonomous systems. *Congr. Numer.*, **30**(3), 265–284.
- Doedel, E. J., Champneys, A. R., Dercole, F., Fairgrieve, T. F., Kuznetsov, Y. A., Oldeman, B., Paffenroth, R., Sandstede, B., Wang, X. & Zhang, C. (2007) *AUTO-07P: Continuation and bifurcation software for ordinary differential equations*.
- Field, M. & Richardson, R. (1992) Symmetry breaking and branching patterns in equivariant bifurcation theory II. *Archive for rational mechanics and analysis*, **120**(2), 147–190.
- Field, M. & Swift, J. W. (1991) Stationary bifurcation to limit cycles and heteroclinic cycles. *Nonlinearity*, **4**(4), 1001.
- Frey, E. (2010) Evolutionary game theory: Theoretical concepts and applications to microbial communities. *Physica A: Statistical Mechanics and its Applications*, **389**(20), 4265–4298.

- Guckenheimer, J. & Holmes, P. (1988) Structurally stable heteroclinic cycles. In *Mathematical Proceedings of the Cambridge Philosophical Society*, volume 103, pages 189–192. Cambridge University Press.
- Hasan, C. R., Osinga, H. M., Postlethwaite, C. M. & Rucklidge, A. M. (2021) Spatiotemporal stability of periodic travelling waves in a heteroclinic-cycle model. *Nonlinearity*, **34**(8), 5576.
- Hawick, K. (2011) Cycles, diversity and competition in rock-paper-scissors-lizard-spock spatial game agent simulations. In *Proceedings on the International Conference on Artificial Intelligence (ICAI)*, page 1. The Steering Committee of The World Congress in Computer Science, Computer.
- Jackson, J. & Buss, L. (1975) Alleopathy and spatial competition among coral reef invertebrates. *Proceedings of the National Academy of Sciences*, **72**(12), 5160–5163.
- Kass, S. & Bryla, K. (1995) *Rock paper scissors Spock lizard*.
- Kerr, B., Riley, M. A., Feldman, M. W. & Bohannan, B. J. (2002) Local dispersal promotes biodiversity in a real-life game of rock–paper–scissors. *Nature*, **418**(6894), 171–174.
- Kirkup, B. C. & Riley, M. A. (2004) Antibiotic-mediated antagonism leads to a bacterial game of rock–paper–scissors in vivo. *Nature*, **428**(6981), 412–414.
- Krupa, M. (1997) Robust heteroclinic cycles. *Journal of Nonlinear Science*, **7**(2), 129–176.
- May, R. M. & Leonard, W. J. (1975) Nonlinear aspects of competition between three species. *SIAM journal on applied mathematics*, **29**(2), 243–253.
- Park, J., Do, Y., Jang, B. & Lai, Y.-C. (2017) Emergence of unusual coexistence states in cyclic game systems. *Scientific reports*, **7**(1), 1–11.
- Podvigina, O. (2013) Classification and stability of simple homoclinic cycles in \mathbb{R}^5 . *Nonlinearity*, **26**(5), 1501.
- Postlethwaite, C. & Rucklidge, A. (2017) Spirals and heteroclinic cycles in a spatially extended rock-paper-scissors model of cyclic dominance. *EPL (Europhysics Letters)*, **117**(4), 48006.
- Postlethwaite, C. M. & Rucklidge, A. M. (2019) A trio of heteroclinic bifurcations arising from a model of spatially-extended Rock–Paper–Scissors. *Nonlinearity*, **32**(4), 1375.
- Proctor, M. R. & Jones, C. A. (1988) The interaction of two spatially resonant patterns in thermal convection. Part 1. Exact 1: 2 resonance. *Journal of Fluid Mechanics*, **188**, 301–335.
- Reichenbach, T., Mobilia, M. & Frey, E. (2007) Mobility promotes and jeopardizes biodiversity in rock–paper–scissors games. *Nature*, **448**(7157), 1046–1049.
- Reichenbach, T., Mobilia, M. & Frey, E. (2008) Self-organization of mobile populations in cyclic competition. *Journal of Theoretical Biology*, **254**(2), 368–383.

- Saad, Y. (2011) *Numerical methods for large eigenvalue problems: revised edition*. Philadelphia, PA: SIAM.
- Sandstede, B. & Scheel, A. (2000) Absolute versus convective instability of spiral waves. *Physical Review E*, **62**(6), 7708.
- Sandstede, B. & Scheel, A. (2020) Spiral waves: linear and nonlinear theory. *arXiv preprint arXiv:2002.10352*.
- Sinervo, B. & Lively, C. M. (1996) The rock–paper–scissors game and the evolution of alternative male strategies. *Nature*, **380**(6571), 240–243.
- Sinervo, B., Miles, D. B., Frankino, W. A., Klukowski, M. & DeNardo, D. F. (2000) Testosterone, endurance, and Darwinian fitness: natural and sexual selection on the physiological bases of alternative male behaviors in side-blotched lizards. *Hormones and Behavior*, **38**(4), 222–233.
- Szczesny, B., Mobilia, M. & Rucklidge, A. M. (2013) When does cyclic dominance lead to stable spiral waves?. *EPL (Europhysics Letters)*, **102**(2), 28012.
- Szczesny, B., Mobilia, M. & Rucklidge, A. M. (2014) Characterization of spiraling patterns in spatial rock-paper-scissors games. *Physical Review E*, **90**(3), 032704.
- Szolnoki, A., Mobilia, M., Jiang, L.-L., Szczesny, B., Rucklidge, A. M. & Perc, M. (2014) Cyclic dominance in evolutionary games: a review. *Journal of the Royal Society Interface*, **11**(100), 20140735.
- Taylor, D. R. & Aarssen., L. W. (1990) Complex competitive relationships among genotypes of three perennial grasses: implications for species coexistence. *The American Naturalist*, **163**(3), 305–327.
- Woods, P. & Champneys, A. (1999) Heteroclinic tangles and homoclinic snaking in the unfolding of a degenerate reversible Hamiltonian–Hopf bifurcation. *Physica D: Nonlinear Phenomena*, **129**(3-4), 147–170.
- Wulff, C. & Schebesch, A. (2006) Numerical continuation of symmetric periodic orbits. *SIAM Journal on Applied Dynamical Systems*, **5**(3), 435–475.